SOILS AND FOUNDATIONS Vol. 47, No. 4, 811–819, Aug. 2007
Japanese Geotechnical Society

EARTH PRESSURE AND SIDEWALL FRICTION ACTING ON AN EMBEDDED FOOTING IN DRY SAND BASED ON CENTRIFUGE TESTS

SHUJI TAMURA[i], TSUYOSHI IMAYOSHI[ii] and TADASHI SAKAMOTO[ii]

ABSTRACT

Earth pressure and sidewall friction acting on an embedded footing are investigated based on dynamic centrifuge tests on a superstructure-footing model that is supported on piles in sand deposits of different densities. For this purpose, a simple method is presented to evaluate not only the earth pressures on the active and passive sides, but also the sidewall friction of an embedded footing. Results show that the total earth thrust, which is defined by the difference in earth pressure between the passive and active sides, and the sidewall friction counter the inertial force transmitted from the superstructure-footing to the pile head. Especially, the total earth thrust in the dense sand case plays an important role in reducing the shear force at pile heads because the difference between the total earth thrust and sidewall friction in the dense sand is greater than that in loose sand.

Key words: centrifuge model test, earth pressure, (embedded footing), friction, pile, sand (**IGC**: E5/E8)

INTRODUCTION

Lateral response of an embedded footing affects pile stress during an earthquake (e.g., Sugimura and Hirade, 1984). Shaking table tests using a polyacrylamide and bentonite soil model (Iiba et al., 2003) showed that the lateral response of an embedded footing is very effective in reducing pile stress. In contrast, Tamura et al. (2002) reported that the lateral response of an embedded footing tends to increase pile stress in liquefied sand based on large-scale shaking table tests. These reports indicate that the evaluation of lateral response of an embedded footing is important for the seismic design of pile foundations in conformity with their performance.

Lateral response of an embedded footing during a three-dimensional earthquake is an extremely complicated phenomen. Therefore, the evaluation of the lateral response for seismic design generally assumes one-dimensional earthquakes. However, little information is available on the lateral response that comprises active and passive side earth pressures, sidewall friction and base friction, even if one-dimensional earthquakes are assumed.

Several studies have examined earth pressure and friction separately. The mechanism of passive earth pressure has been investigated based on the horizontal loading of a vertical retaining wall, which moved toward dry sand (Wada et al., 1998; Fang et al., 2002). Several theories have been proposed for evaluating seismic earth pressure acting on a retaining wall (e.g., Zhang et al., 1998; Koseki et al., 1998). The friction between dry sand and metal surfaces was investigated in detail using laboratory tests (Yoshimi and Kishida, 1981; Uesugi and Kishida, 1986). The friction between sidewall and dry sand with relative densities (D_r) of 90% and 60% was also evaluated based on lateral static loading centrifuge tests (Nagao et al., 1997).

Several studies have assessed earth pressure and friction acting simultaneously on an embedded footing. The relative contributions of the base, sidewall and active/passive side of an embedded footing in dry sand with $D_r = 75\%$ were evaluated based on cyclic lateral loading centrifuge tests (Gadre and Dobry, 1998). That study showed that the contribution of the passive side accounts for more than half of the total lateral capacity of the embedded footing. Effects of an embedded footing on pile stress were investigated using shaking table tests with a silicone soil model (Imaoka et al., 1998). Results indicated that the lateral response of an embedded footing reduces pile stress remarkably in the frequency range near the natural frequency of the superstructure; in addition, the contribution of the sidewall friction to the total lateral capacity was 15–20%. However, knowledge of earth pressure and friction during a large earthquake and the effects of earth pressure and friction on pile stress remain limited.

The objectives of this investigation are: 1) to evaluate earth pressure and sidewall friction acting on an embedded footing during a large earthquake, 2) to examine the effects of soil density on development of earth pressure and sidewall friction, 3) to study the effects of earth pressure and sidewall friction on the shear force at pile heads. For this purpose, dynamic centrifuge tests on a superstructure-footing model that is supported on piles in sand

[i] Associate Professor, Disaster Prevention Research Institute, Kyoto University, Japan (tamura@sds.dpri.kyoto-u.ac.jp).
[ii] Graduate Student, Kyoto University, Japan.
The manuscript for this paper was received for review on October 23, 2006; approved on March 26, 2007.
Written discussions on this paper should be submitted before March 1, 2008 to the Japanese Geotechnical Society, 4-38-2, Sengoku, Bunkyo-ku, Tokyo 112-0011, Japan. Upon request the closing date may be extended one month.

deposits of different densities were performed. In addition, a simple method is presented to evaluate not only earth pressures on active and passive sides, but also sidewall friction of an embedded footing.

EVALUATION OF SIDEWALL FRICTION

A simple method is presented to evaluate the sidewall friction of an embedded footing. Figure 1 depicts a schematic figure showing forces acting on pile heads, an embedded footing, and a superstructure. The sum of the shear forces at pile heads, Q, can be expressed as

$$Q = P_{et} + P_{fs} + P_{fb} + F_{is} + F_{if} \quad (1)$$

where P_{et} = total earth thrust, P_{fs} = sidewall friction, P_{fb} = base friction, F_{is} = superstructure inertia and F_{if} = footing inertia. The total earth thrust, P_{et} can be evaluated as

$$P_{et} = P_R - P_L \quad (2)$$

where P_R = earth thrust acting on the footing's right side, and P_L = earth thrust acting on the footing's left side. The sidewall friction is given as

$$P_{fs} = Q - P_{et} - P_{fb} - F_{is} - F_{if} \quad (3)$$

If the base friction is neglected, the sidewall friction can be evaluated by measurements of the shear force at the pile heads, the total earth thrust, and the inertial force of the superstructure and footing.

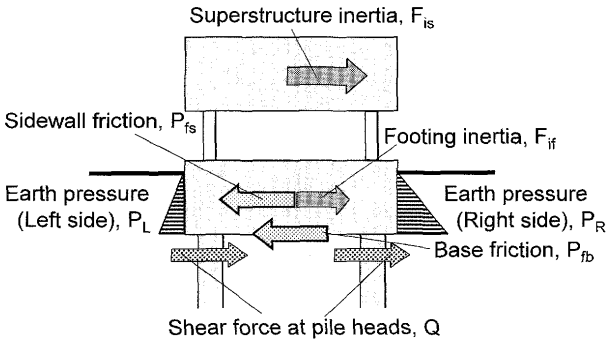

Fig. 1. Forces acting on superstructure, embedded footing and pile heads

CENTRIFUGE TESTS PERFORMED

Test Cases

A series of dynamic centrifuge tests was performed at 40g centrifugal acceleration using the Disaster Prevention Research Institute, Kyoto University geotechnical centrifuge. A piles-footing-superstructure model was prepared in a laminar shear box with inner dimensions of 450 mm (length) × 150 mm (width) × 200 mm (height). The soil used for dry sand deposit was Toyoura sand. Four centrifuge tests that were performed are shown in Fig. 2 and Table 1. In Case 1, the footing was not embedded in the sand. Accordingly, the earth pressure and sidewall friction do not act on the footing. In Case 2, the footing was embedded in the sand with $D_r = 95\%$ and sponges were set between the footing sidewall and the laminar shear box. Consequently, the earth pressure acts on the footing, whereas the sidewall friction acts only slightly on the footing. In Cases 3 and 4, the footing was embedded respectively in the dense sand with $D_r = 95\%$ and in the loose sand with $D_r = 45\%$, thereby, the sidewall friction and the earth pressure act on the footing. The sand layers were prepared by pluviating dry sand in Cases 1 and 4 and were then compacted to $D_r = 95\%$ in Cases 2 and 3.

Piles-Footing-Superstructure Model

A sketch and conditions of a piles-footing-superstructure model are shown respectively in Fig. 3 and Table 2. A 2 × 2 pile model was used for all tests. The pile was modeled with an 8 mm diameter round brass bar. The bending stiffness, EI of the pile model was 2.65×10^{-5} MNm^2. The lid-shaped footing was modeled with a rigid brass of dimensions 104 mm (shaking direction) × 88 mm

Table 1. Centrifuge tests performed

	Earth Presuure	Sidewall Friction	Relative Density	Input Motion Dis.
Case 1	No	No	75%	3 mm
Case 2	Yes	No	95%	2 mm
Case 3	Yes	Yes	95%	4.7 mm
Case 4	Yes	Yes	45%	4.7 mm

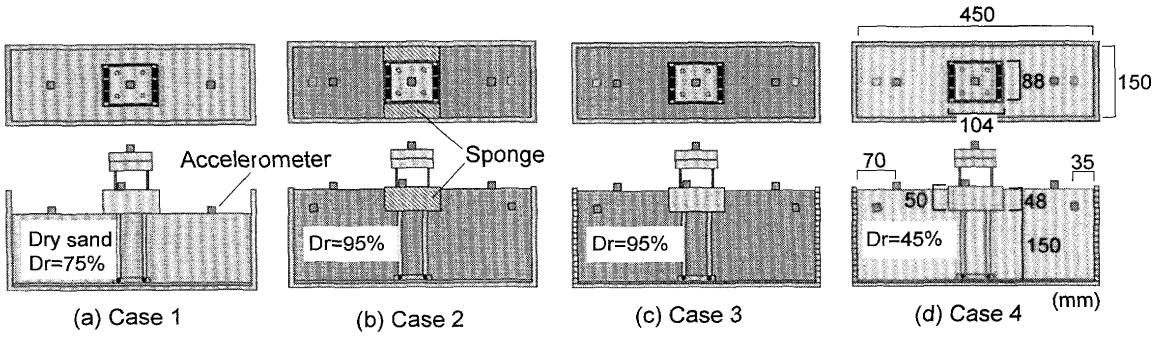

Fig. 2. Setup for centrifuge tests on piles-footing-superstructure model

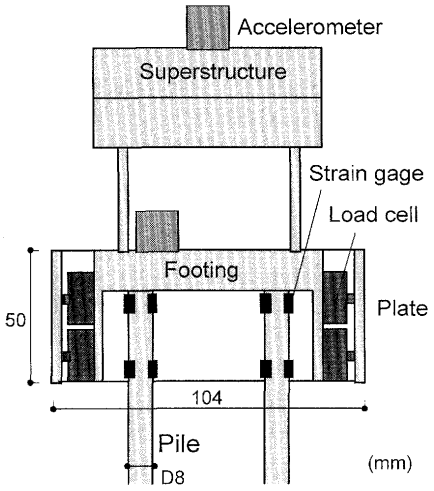

Fig. 3. Piles-footing-superstructure model

Table 2. Conditions of piles-footing-superstructure system in prototype and model scale

		Unit	Prototype	Model
Pile	Length	m	7.2	0.18
	Diameter	m	0.32	0.008
	E·I	MNm^2	52.9	2.06×10^{-5}
Footing	Mass	kg	102, 400	1.6
	Length (L×B×H)	m	4.16×3.52 ×2.00	0.104×0.088 ×0.050
Structure	Mass	kg	134, 400	2.1
	Natural frequency	Hz	2.5	100

(width) × 50 mm (height). The footing is embedded in dry sand 48 mm thick in Cases 2–4. The pile heads were linked rigidly with the upper plate of the footing model and their tips were connected to the laminar shear box by hinges. The strain gauges at the pile heads were not in contact with the soil. Therefore, the shear force at the pile heads Q, calculated by differentiation of the strain, was measured accurately, independent of the soil effects. Additionally, the footing base friction P_{fb} is negligible. A plate supported by three small load cells was set up on the right and left sides of the footing to evaluate earth pressure acting on the footing, P_R and P_L. The surface of the footing modeled with brass is smoother than that of a prototype footing. For that reason, a fine grade of sandpaper (#800) was pasted on the sidewalls, the right and left sides of the footing. The superstructure was modeled with rigid brass. The natural frequency and the damping constant of the superstructure under the fixed footing condition are 104 Hz and 2 %, respectively.

Horizontal acceleration of the superstructure-footing and soil, the bending moment at the pile heads, and the earth pressure acting on the right and left sides of the footing were measured. The superstructure inertia F_{is} and

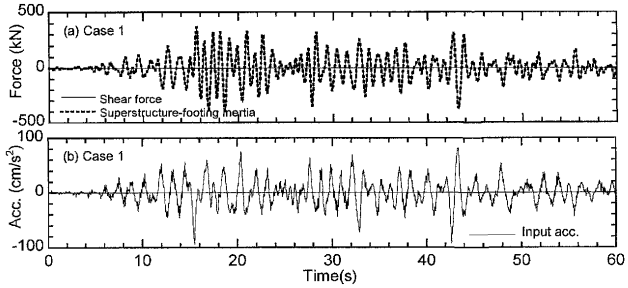

Fig. 4. Time histories in Case 1

the footing inertia F_{if} can be evaluated by their mass and the measured acceleration. The total earth thrust P_{et} and sidewall friction P_{fs} can be evaluated, respectively, using Eqs. (2) and (3). All tests were excited by RINKAI92 (Japan Building Disaster Prevention Association, 1992), which is one-dimensional (horizontal) synthesized ground motion expected for the Tokyo Bay area. All data presented in the following sections are of prototype scale.

TEST RESULTS

Test Results in Cases 1 and 2

Case 1 was performed to confirm the accuracy of the measurement of the superstructure and footing inertia and the shear force at the pile heads. Figure 4 shows the time histories of the input acceleration, the sum of the shear force at the pile heads, and the superstructure-footing inertia defined by the sum of the superstructure inertia and the footing inertia in Case 1. The superstructure-footing inertia shows fairly good agreement with the shear force, suggesting that the superstructure and footing inertia and the shear force at the pile heads can be evaluated accurately.

Case 2 was performed to confirm the accuracy of the measurement of the earth pressure evaluated by the load cells. Figure 5 shows the time histories of the input acceleration, the superstructure-footing inertia, the sum of the shear force at the pile heads, the total earth thrust evaluated by the load cells, the difference between the superstructure-footing inertia and the shear force at the pile heads in Case 2. The superstructure-footing inertia amplitude was apparently larger than the shear force amplitude. The difference between the superstructure-footing inertia and the shear force gives fairly good agreement with the total earth thrust evaluated by the load cells, suggesting that the earth pressure can be evaluated accurately by the load cells. The two test results described above suggest that the total earth thrust and the sidewall friction can be evaluated respectively using Eqs. (2) and (3).

Test Results in Cases 3 and 4

Cases 3 and 4 were performed to evaluate the earth pressure acting on the footing and the sidewall friction. Figures 6 and 7 show the acceleration time histories of the superstructure, footing, ground surface, and input motion, as well as the superstructure-footing inertia, shear

force at the pile heads, total earth thrust, and sidewall friction in Cases 3 and 4, respectively. The maximum amplitude of the input motion, the footing, superstructure, and ground surface acceleration in Case 3 resemble those of Case 4. The maximum amplitudes of the total earth thrust and sidewall friction in Case 3 were larger than those of Case 4. It is noteworthy that the shear force amplitude at the pile heads in Case 3 tended to be smaller than that in Case 4, even though the superstructure-footing inertia amplitude in Case 3 is similar to that in Case 4.

The predominant frequencies of the ground surface acceleration during the shaking are 1.04 Hz and 0.65 Hz in Cases 3 and 4, respectively. The natural frequency of the superstructure under the fixed footing condition is 2.6 Hz in both cases. Therefore, the natural frequency of the superstructure is higher than the predominant frequency of the ground surface in both cases.

Displacement of the footing and soil were calculated by double integration of the acceleration. Figures 8(a), (b) show the time histories of soil displacement at left and right sides of the footing, which are the average of displacements at the ground surface and the footing bottom level as shown in Fig. 2. The soil displacement measured by the both sides of the footing show fairly good agreement, suggesting that the displacement is independent of the footing response. Thus, we assumed that the average of soil displacement at left and right sides of the footing

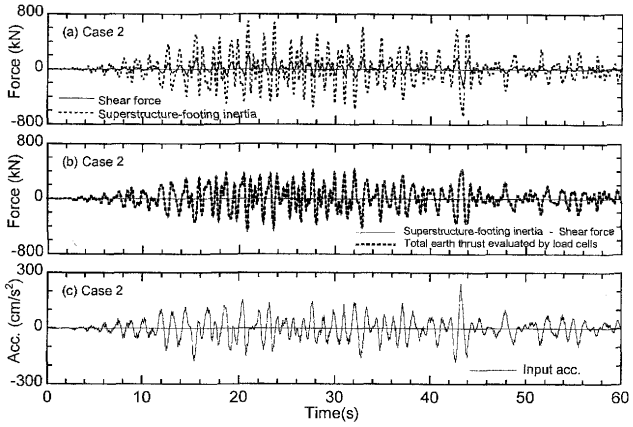

Fig. 5. Time histories in Case 2

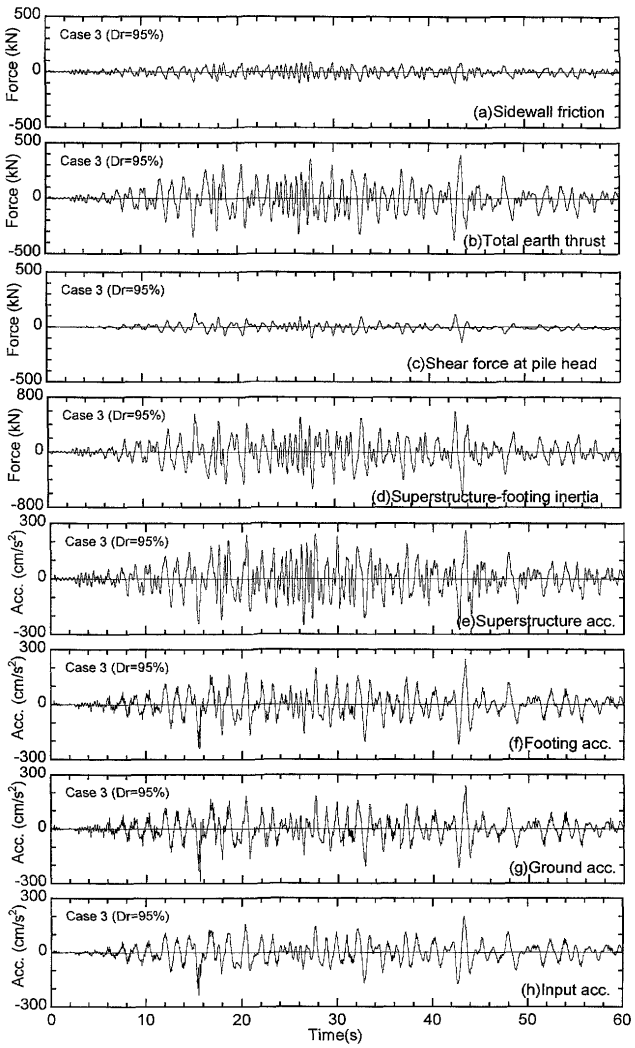

Fig. 6. Time histories in Case 3 (Dense sand)

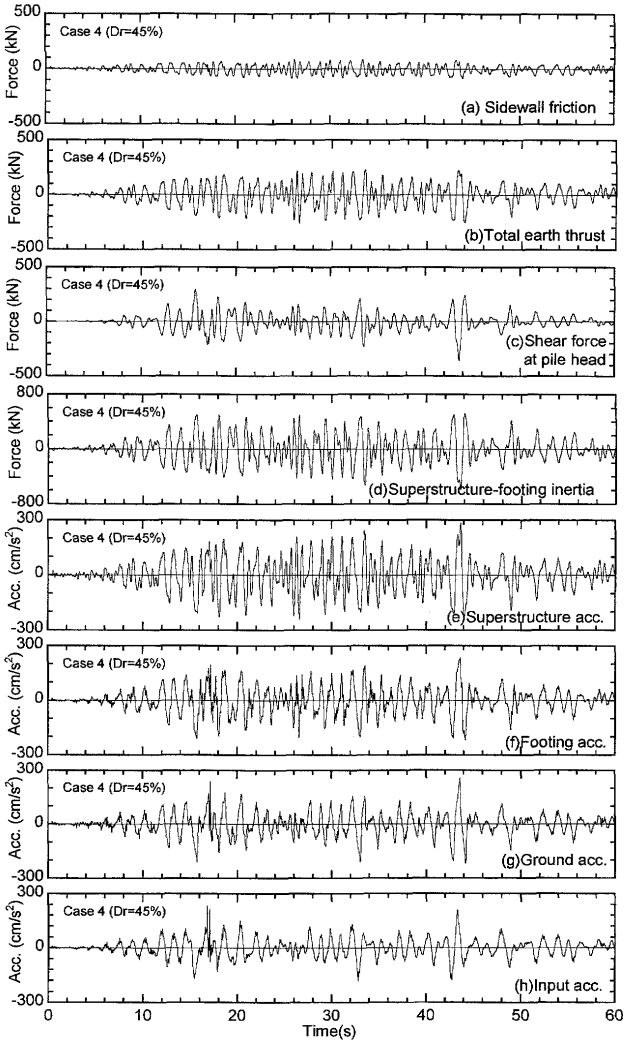

Fig. 7. Time histories in Case 4 (Loose sand)

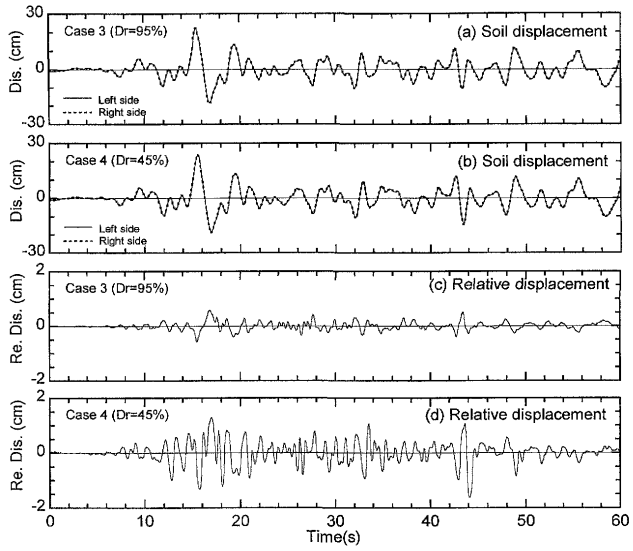

Fig. 8. Time histories of displacement in Cases 3 and 4

to be free field. Figures 8(c), (d) show the time history of the relative displacement between the footing and the soil, in which the soil displacement is the average of displacement at left and right sides of the footing. The relative displacement amplitude in Case 3 is smaller than that in Case 4.

EFFECTS OF EARTH PRESSURE AND FRICTION ON SHEAR FORCE AT THE PILE HEADS

Relation between Superstructure-footing Inertia and Total Earth Thrust and Sidewall Friction

Relations between the superstructure-footing inertia and the total earth thrust in Cases 3 and 4 are shown in Fig. 9 to elucidate the effects of the total earth thrust on the shear force at the pile heads. The data in the first and third quadrants show that the total earth thrust is in phase with the superstructure-footing inertia, whereas those in the second and fourth quadrants show that the total earth thrust is out of phase by 180° with the superstructure-footing inertia. The total earth thrust in either case tends to be out of phase by 180° with the superstructure-footing inertia. Furthermore, the total earth thrust amplitude increases in relation to the superstructure-footing inertia amplitude. These facts suggest that the total earth thrust, generated as the reaction force of the superstructure-footing inertia, counters the inertial force transmitted from the superstructure-footing to the pile heads.

The relations between the superstructure-footing inertia and the sidewall friction in Cases 3 and 4 are shown in Fig. 10. The sidewall friction also tends to be out of phase by 180° with the superstructure-footing inertia and its amplitude increases in close relation to the superstructure-footing inertia. These indicate that the sidewall friction, generated as a reaction force of the superstructure-footing inertia, counters the inertial force transmitted from the superstructure-footing to the pile heads.

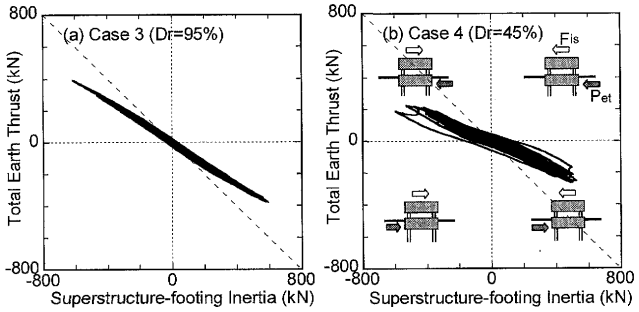

Fig. 9. Relation between superstructure-footing inertia and total earth thrust

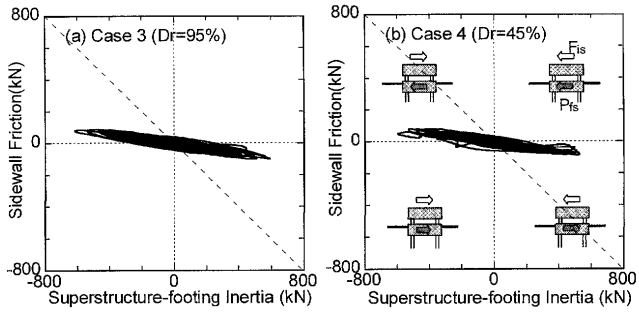

Fig. 10. Relation between superstructure-footing inertia and sidewall friction

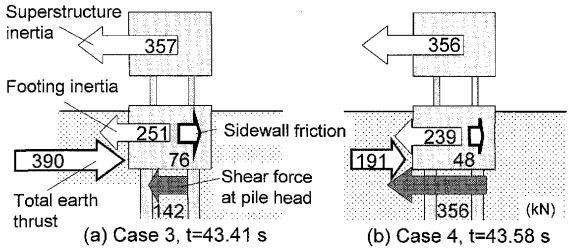

Fig. 11. Forces acting on piles-footing-superstructure system

Forces Acting on the Footing and Superstructure at Maximum Shear Force at the Pile Heads

Figure 11 shows forces acting on the piles-footing-superstructure system at time $t = 43.41$ s in Case 3 and at $t = 43.58$ s in Case 4, when the shear force at the pile heads became maximum. The superstructure inertia and the footing inertia in Case 3 are almost equal to those in Case 4. The superstructure-footing inertia in either case is greater than the shear force at the pile heads because the total earth thrust and sidewall friction counter the inertial force transmitted to the pile heads. The total earth thrust amplitudes of Cases 3 and 4 are 390 kN and 191 kN, which are, respectively, 64% and 32% of the superstructure-footing inertia. The sidewall friction amplitudes in Cases 3 and 4 are 76 kN and 48 kN, which are, respectively, 13% and 8% of the superstructure-footing inertia. Consequently, the shear force amplitude in Cases 3 is less than half of that in Case 4. These indicate that the total earth thrust plays an important role in reduction of the

shear force at pile heads in the dense sand case.

EFFECTS OF SOIL DENSITY ON EARTH PRESSURE AND FRICTION

Relation between Relative Displacement and Total Earth Thrust

Figure 12 shows the relation between the total earth thrust and the relative displacement between the soil and footing in Cases 3 and 4. The total earth thrust amplitude in Case 3 is larger than that in Case 4, although the relative displacement in Case 3 is smaller than that in Case 4.

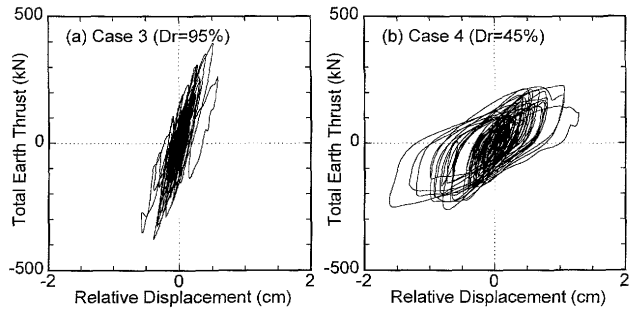

Fig. 12. Relation between relative displacement and total earth thrust

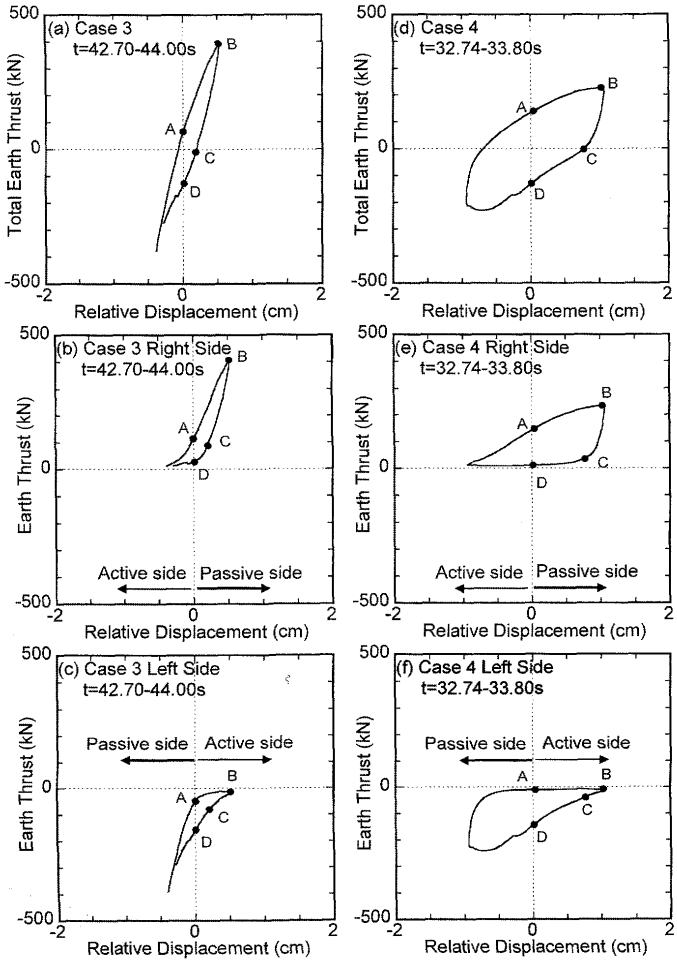

Fig. 13. Relations between relative displacement and total earth thrust, earth thrust acting on right side and on left side of embedded footing

To elucidate the mechanism of the total earth thrust, Fig. 13 shows the hysteresis loops of the total earth thrust, the earth thrust acting on the right side, and the left side of the footing in Cases 3 and 4, when the total earth thrust became the maximum. The right side is a passive side and the left side is an active side when the relative displacement is greater than zero. The hysteresis loop of the total earth thrust is separable into three processes, A→B, B→C, and C→D, as shown in the figure. First, the total earth thrust during reloading A→B is caused mainly by the passive side earth pressure because the passive side (Right side) earth thrust increases with the relative displacement; the active side (Left side) earth thrust is extremely small. Secondly, the total earth thrust during unloading B→C is also caused mainly by the passive side earth pressure because the passive side earth thrust is larger than the active side earth thrust. Finally, the total earth thrust during unloading C→D is caused mainly by the active side earth pressure because the active side earth thrust increases with the relative displacement and the passive side earth thrust is extremely small. These indicate that the total earth thrust during reloading is caused mainly by the passive side earth pressure. In contrast, the total earth thrust during unloading is caused by both the passive and active side earth pressures.

To elucidate the effects of soil density on the development of the total earth thrust, Fig. 14 presents a comparison of the relative displacement and the peak value of the total earth thrust in Cases 3 and 4. The total earth thrust in Case 3 increases more rapidly than that in Case 4 with increasing relative displacement. The rapid increase in the total earth thrust in the dense sand agrees with test results of the horizontal loading of a vertical retaining wall, which moved toward dry sand (Wada et al., 1998; Fang et al., 2002). The values of the maximum total earth thrust are, respectively, 394 kN and 261 kN in Cases 3 and 4. The experimental earth pressure coefficients K_h, as defined by the following equation, are 3.8 and 2.8, respectively, in Cases 3 and 4.

$$K_h = P_{max}/(\gamma H^2 B/2) \quad (4)$$

In this equation, P_{max} is the maximum total earth thrust, γ is the unit weight of soil, H is the embedment depth of the

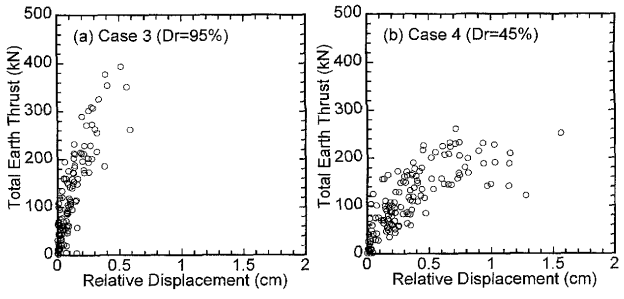

Fig. 14. Relation between relative displacement and total earth thrust peak

footing, and B denotes the footing width. The theoretical passive earth pressure coefficients K_p, which are estimated with the Coulomb theory, are 12.5 and 5.7, respectively, in Cases 3 and 4 if we assume that the inertial friction angle of soil ϕ is 45° in Case 3 and 35° in Case 4 and that the sand-wall friction angle δ is $\phi/3$. The experimental earth pressure coefficients are smaller than the theoretical coefficients, indicating that the experimental earth pressure did not reach the passive earth pressure in both cases. This discrepancy pertains because the relative displacement is less than the displacement required to develop the passive state that is reported for 0.05 H for dense sand and 0.16 H for medium sand (Wada et al., 1998), and 0.015 H for dense sand and 0.03 H for medium sand (Fang et al., 2002).

Relation between Relative Displacement and Sidewall Friction

Figure 15 shows the relation between the relative displacement and the sidewall friction in Cases 3 and 4. The amplitude of the sidewall friction in Case 3 is slightly larger than that in Case 4, although the relative displacement in Case 3 is apparently smaller than that in Case 4. The sidewall friction in the loose sand exhibits highly nonlinear behavior.

The relations between the relative displacement and the peak value of the sidewall friction in Cases 3 and 4 are shown in Fig. 16 to portray the effects of soil density on the development of sidewall friction. The sidewall friction in Case 3 increases more rapidly than that in Case 4 with increasing relative displacement. The values of the ultimate sidewall friction are, respectively, 99.5 kN and 85.0 kN in Cases 3 and 4. The ultimate sidewall friction depends on normal stress, i.e. lateral pressure acting on the sidewall, but the lateral pressure was not measured in this study. The friction coefficients μ are, respectively, 1.02 and 0.78 in Cases 3 and 4 if we assume that the respective coefficients of earth pressure at rest K_0 are 0.4 and 0.5. The friction coefficient in Case 3 is greater than 1.0. This is probably because that the lateral pressure acting on the sidewall increases during shaking. The friction coefficient depends on the shear failure of the sand mass when the material surface is rough (Uesugi and Kishida, 1986). Therefore, the friction coefficient of dry sand can be evaluated approximately using the following equation based on Coulomb's failure criterion (Nagao et al., 1997).

$$\mu = \tan\phi \tag{5}$$

The theoretical friction coefficients μ are, respectively, 1.00 and 0.70 in Cases 3 and 4 by Eq. (5) if we assume that inertial friction angles ϕ are 45° and 35°, respectively. The theoretical friction coefficients agree with the test results, indicating that the seismic friction coefficient is also evaluated approximately by Eq. (5). The friction in either case reaches its greatest value when the displacement is about 0.3–0.4 cm. The relative displacement amplitude in Case 4 tends to be larger than the yield displacement. As a result, the sidewall friction in Case 4 exhibits nonlinearity as shown in Fig. 15.

It has been reported variously that the yield displacement of friction is 0.05–0.18 cm (Uesugi and Kishida, 1986) and 0.02–0.15 cm (Nagao et al., 1997), which depends on the material's roughness and the soil's relative density. The yield displacement in this study, which is 40 times as large as the measured displacement in model scale is bit larger than that in the previous studies. The yield displacement depends on a shear band along the sidewall. The shear band is, however, not necessary satisfied with the centrifuge scaling law, because of the grain size effects (Tatsuoka et al., 1997). If the grain size effects can not be neglected, the displacement based on the centrifuge scaling law tends to be overestimated (Garnier and König, 1998), suggesting that the possibility that actual yield displacement is smaller than 0.3–0.4 cm.

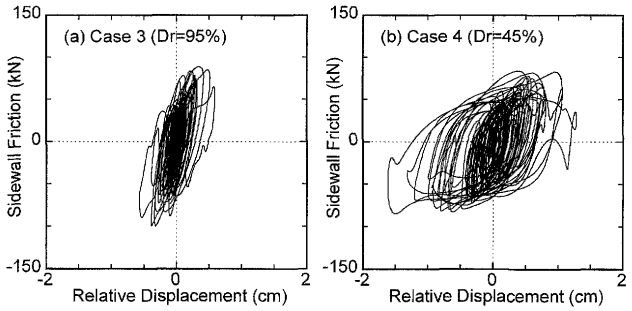

Fig. 15. Relation between relative displacement and sidewall friction

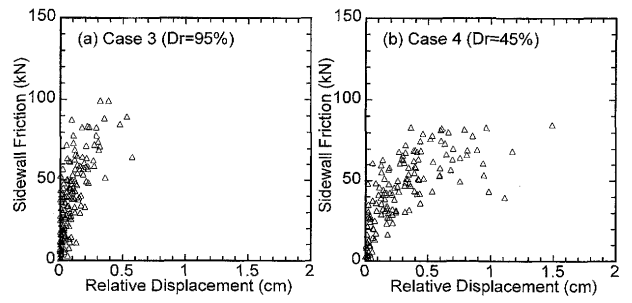

Fig. 16. Relation between relative displacement and sidewall friction peak

Comparison of Total Earth Thrust and Sidewall Friction

Figure 17 portrays a comparison of the total earth thrust peaks and sidewall friction peaks only when the respective relative displacement is greater than the previous maximum value. Considering that the footing model plane is a rectangle, the total earth thrust and the sidewall friction amplitude were divided by 3.52 m in the footing width and by 4.16 m in the footing length. The difference between the total earth thrust and the sidewall friction amplitude is small at extremely small relative displacement. The total earth thrust increases with increasing relative displacement, indicating that the earth pressure did not reach the passive earth pressure. On the other hand, the sidewall friction remains constant or decreases when the relative displacement is greater than the yield dis-

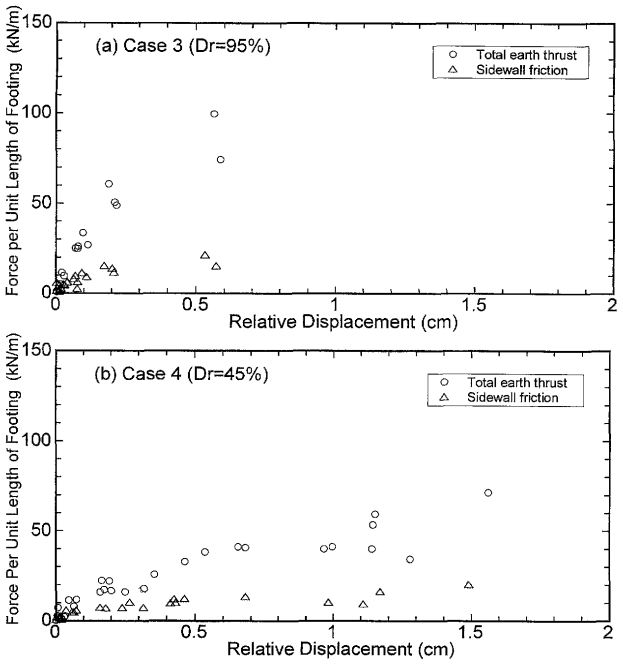

Fig. 17. Relation between relative displacement and total earth thrust and sidewall friction peaks that exceed previous maximum relative displacement

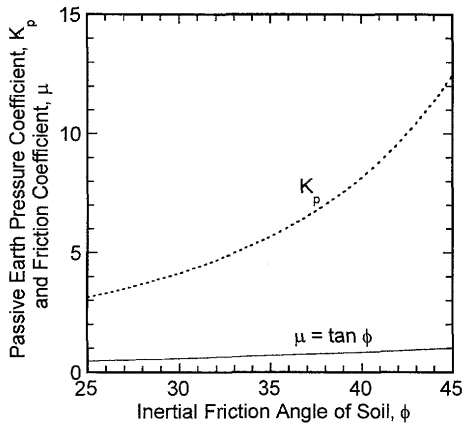

Fig. 18. Relation between inertial friction of soil and passive earth pressure coefficient K_p and friction coefficient μ

placement, 0.3–0.4 cm. This yield displacement of the sidewall friction is smaller than the displacement required to develop passive earth pressure reported by the previous studies (Wada et al., 1998; Fang et al., 2002). Therefore, the difference between the total earth thrust and the sidewall friction amplitude becomes larger as the relative displacement increases. This tendency is considerably strong in Case 3.

To elucidate the effects of relative density of soil, the relation between the inertial friction angle of soil and the theoretical passive earth pressure coefficient K_p and friction coefficient μ is depicted in Fig. 18. The theoretical passive earth pressure coefficient and friction coefficient were calculated using the Coulomb theory with $\delta = \phi/3$ and Eq. (5), respectively. The passive earth pressure coefficient increases exponentially with the increasing inertial friction angle of the soil. In contrast, the friction coefficient increases linearly with the increasing inertial friction angle, which indicates that the earth pressure in dense sand contributes more to the lateral response of the embedded footing than that in loose sand.

CONCLUSIONS

A simple method is presented to evaluate not only the earth pressures on the active and passive sides but also the sidewall friction of an embedded footing. The earth pressure and sidewall friction are investigated based on dynamic centrifuge tests on a superstructure-footing model that is supported on piles in a sand deposit of different densities: $D_r = 95\%$ and $D_r = 45\%$. The following conclusions are drawn:

(1) The total earth thrust and sidewall friction counter the inertial force transmitted from the superstructure-footing to the pile heads. Especially, the total earth thrust in the dense sand case plays an important role in reducing the shear force at pile heads because the difference between the total earth thrust and sidewall friction in the dense sand is greater than that in the loose sand.

(2) The theoretical passive earth pressure coefficient increases exponentially with the increasing inertial friction angle of soil. On the other hand, the theoretical friction coefficient increases linearly with the increasing inertial friction angle. This difference in relationships indicates that the difference between the passive earth pressure and the sidewall friction increases concomitant with the inertial friction angle of soil.

(3) The sidewall friction in either case reaches its greatest value when the relative displacement is 0.3–0.4 cm, which is smaller than the displacement required to develop passive earth pressure. Therefore, the difference between the total earth thrust and the sidewall friction amplitude increases concomitant with the relative displacement.

(4) The amplitude of the total earth thrust in the dense sand case increases more rapidly than that in the loose sand case with increasing relative displacement between the footing and soil.

(5) The total earth thrust during reloading is affected mainly by the passive side earth pressure, whereas that during unloading is affected by both the passive and active side earth pressures.

ACKNOWLEDGMENTS

The authors thank Prof. K. Tokimatsu, Tokyo Institute of Technology for discussion of the test results and Mr. M. Hatsuyama, a graduate student of Kyoto University, for assistance with the centrifuge tests. This study was conducted with the financial support of Grant-in-Aid for Scientific Research No. 14301 from the Ministry of

Education, Culture, Sports, Science and Technology of Japan.

REFERENCES

1) Fang, Y. S., Ho, Y. C. and Chen, T. J. (2002): Passive earth pressure with critical state concept, *Journal of Geotechnical Engineering*, ASCE, **128**(8), 651–659.
2) Gadre, A. and Dobry, R. (1998): Lateral cyclic loading centrifuge tests on square embedded footing, *Journal of Geotechnical and Geoenvironmental Engineering*, ASCE, **124**(11), 1128–1138.
3) Garnier, J. and König, D. (1998): Scale effects in piles and nails loading tests in sand, *Proc. International Conference Centrifuge 98*, 205–210.
4) Iiba, M., Tamori, S. and Kitagawa, Y. (2003): Fundamental characteristics on seismic effect to pile foundation by shaking table test for model of building-soil interaction system, *Journal of Struct. Constr. Eng.*, AIJ, (566), 29–36 (in Japanese).
5) Imaoka, K., Tokutake, S., Aoyama, K., Fukuwa, N., Iiba, M. and Taga, N. (1998): Dynamic embedment effects using silicone soil model, *Proc. 10th Earthquake Engineering Symposium*, 1653–1658 (in Japanese).
6) Japan Building Disaster Prevention Association (1992): Study on input ground motion for dynamic design, *Committee Report* (in Japanese).
7) Koseki, J., Tatsuoka, F., Munaf, Y., Tateyama, M. and Kojima, K. (1998): A modified procedure to evaluate active earth pressure at high seismic loads, *Soils and Foundations*, Special Issue on Geotechnical Aspects of the 1995 Hyogoken Nambu Earthquake, (2), 209–216.
8) Nagao, T., Watanabe, T., Wakame, Y. and Majima, M. (1997): Fundamental study on the earth pressure acting on the basement wall-Behavior of friction acting on basement wall-, *Report of Taisei Research Institute*, **30**, 205–210 (in Japanese).
9) Sugimura, Y. and Hirade, T. (1984): Experimental study on reduction effect of horizontal force due to embedment of foundation, *Summaries of Technical Papers of Annual Meeting*, AIJ, Structures II, 2409–2410 (in Japanese).
10) Tamura, S., Tokimatsu, K., Uchida, A., Funahara, H. and Abe, A. (2002): Relation between seismic earth pressure acting on embedded footing and inertial force based on liquefaction test using large scale shear box, *Journal of Struct. Constr. Eng.*, AIJ, (559), 129–134 (in Japanese).
11) Tatsuoka, F., Goto, S., Tanaka, T., Tani, K. and Kimura, Y. (1997): Particle size effects on bearing capacity of footing on granular material, *Proc. IS-NAGOYA*, 133–138.
12) Uesugi, M. and Kishida, H. (1986): Influential factors of friction between steel and dry sands, *Soils and Foundations*, **26**(2), 33–46.
13) Wada, S., Kouda, M. and Enami, A. (1998): Experimental study on passive earth pressure, Part 1 The experimental device and an example of the passive earth pressure test by the device, *Journal of Struct. Constr. Eng.*, AIJ, (503), 69–76 (in Japanese).
14) Yoshimi, Y. and Kishida, T. (1981): A ring torsion apparatus for evaluating friction between soil and metal surfaces, *Geotechnical Testing Journal*, GTGODJ, **4**(4), 145–152.
15) Zhang, J.-M., Shamoto, Y. and Tokimatsu, K. (1998): Seismic earth pressure theory for retaining walls under any lateral displacement, *Soils and Foundations*, **38**(2), 143–163.